

Cite this: *RSC Adv.*, 2019, **9**, 5091

Computational investigations into the structural and electronic properties of Cd_nTe_n ($n = 1\text{--}17$) quantum dots†

Muhammad Imran, ^a Muhammad Jawaad Saif, ^{*a} Aleksey E. Kuznetsov, ^b Nazeran Idrees, ^c Javed Iqbal ^d and Asif Ali Tahir ^e

Size-tunability of the electronic and optical properties of semiconductor quantum dots and nanoclusters is due to the quantum size effect, which causes variations in the electronic excitations as the particle boundaries are changed. Recently, CdSe and CdTe quantum dots have been used in energy harvesting devices. Despite these promising practical applications, a complete understanding of the electronic transitions associated with the surfaces of the nanoparticles is currently lacking and is difficult to achieve experimentally. Computational methods could provide valuable insights and allow us to understand the electronic and optical properties of quantum dots and nanoclusters. Hollow cage and endohedral or core–shell cage structures for Cd_nTe_n clusters have been reported before. We have performed systematic density functional theory (DFT) studies on the structure and electronic properties of the Cd_nTe_n ($n = 1\text{--}17$) clusters. As the number of atoms increases in the Cd_nTe_n clusters, the predicted geometries change from simple planar structures to more complicated 3D-structures. Two classes of the most stable structures were elucidated for clusters with $n = 10\text{--}17$: (i) hollow cage structures with an empty center; and (ii) endohedral or core–shell cage structures with one or more atoms inside the cage. Noticeably higher highest occupied molecular orbital (HOMO)-lowest unoccupied molecular orbital (LUMO) gaps were observed for the hollow cage isomers as compared to the core–shell structures. The highest occupied molecular orbitals of all of the clusters studied were shown to be localized on the surface of the cage for the hollow cage structures, while in the case of the core–shell structures, the HOMO electron densities were found to be distributed both on surface and the interior of the structures. Most of the small size clusters Cd_nTe_n ($n = 2\text{--}9$) showed minimal values for the dipole moments (close to zero) owing to the highly ordered and symmetric configurations of these structures. For isomers of the larger clusters ($n = 10\text{--}17$), it was observed that the core–shell structures have higher values for the dipole moments than the hollow cage species because of the highly symmetric structures of the hollow cages. Core–shell cage structures exhibited lower polarizability than the respective hollow cage structures.

Received 17th November 2018

Accepted 22nd January 2019

DOI: 10.1039/c8ra09465a

rsc.li/rsc-advances

1 Introduction

Semiconductor quantum dots have attracted significant interest owing to their tunable electronic and optical properties as a result of variations in the size, shape and surface chemistry of the particles.¹ These semiconductor nanomaterials are

becoming increasingly important owing to their potential applications in electronic and optoelectronic devices such as solar cells, electro-optical modulators, photodetectors, light emitting diodes and sensors.^{1–13} Size-tunability of the electronic and optical properties of semiconductor quantum dots and nanoclusters is due to the quantum size effect, which causes

^aDepartment of Applied Chemistry, Government College University Faisalabad, Pakistan. E-mail: jawwadsaif@gmail.com

^bDepartamento de Química, Universidad Técnica Federico Santa María, Av. Santa María 6400, Vitacura, Santiago, Chile

^cDepartment of Mathematics, Government College University Faisalabad, Pakistan

^dDepartment of Chemistry, University of Agriculture, Faisalabad, Pakistan

^eEnvironment and Sustainability Institute, University of Exeter, Penryn Campus, TR10 9FE, UK

† Electronic supplementary information (ESI) available: Supporting information contains Fig. S1. HOMO and LUMO of the most stable lowest-energy clusters Cd_nTe_n ($n = 1\text{--}9$); Fig. S2. HOMO and LUMO of the

lowest-energy core–shell cage and hollow cage structures Cd_nTe_n ($n = 10\text{--}17$); Fig. S3. Plots of the LUMO+1 for clusters Cd_nTe_n ($n = 1\text{--}17$); Fig. S4. Plots of the LUMO+2 for clusters Cd_nTe_n ($n = 1\text{--}17$); Table S1. The binding energy (E_b) in eV per CdTe unit, point groups, HOMO values, LUMO values and HOMO–LUMO gaps calculated using the B3LYP/Lanl2dz level of theory for the lowest energy optimized structures of Cd_nTe_n ($n = 1\text{--}17$), the hollow cage and endohedral (core–shell) cage structures ($n = 10\text{--}17$) and Table S2. The binding energy (E_b) in eV per CdTe unit, point groups calculated using the MP2/Def2-TZVP level of theory for the lowest energy optimized structures of Cd_nTe_n ($n = 1\text{--}17$), the hollow cage and endohedral (core–shell) cage structures ($n = 10\text{--}17$). See DOI: 10.1039/c8ra09465a



variations in the electronic excitations as the particle boundaries are changed.¹⁴ Recently, CdSe and CdTe quantum dots have been used in energy harvesting devices, for example, quantum dot-sensitized solar cells.^{6–10} Despite the promising practical applications of semiconductor quantum dots and nanoclusters, a complete understanding of the electronic transitions associated with the surface of nanoparticles is currently lacking and is difficult to achieve experimentally. However, computational methods could provide valuable insights to allow researchers to understand the electronic and optical properties of quantum dots and nanoclusters.¹⁵ This understanding of the electronic structure and a knowledge of how to manipulate it has great importance as far as practical applications are concerned. Numerous theoretical studies have been conducted to understand the electronic properties of CdSe and CdTe nanoclusters. Hybrid nanostructures have been developed combining graphene with CdTe quantum dots to tune the band gap of the system.¹⁶ A similar study was conducted with a hybrid nanostructure composed of a CdTe nanotube and fullerene to engineer the electronic structure and band gap of the nanocomposite.¹⁷ In one of the earliest computational studies on CdTe nanoclusters, Bhattacharya and Kshirsagar conducted a density functional theory (DFT) calculations for CdTe nanoclusters to determine their structural and electronic properties.¹⁸ The search for geometrical structures of Cd_nTe_n clusters remains the focus of many researchers and various structures containing a small number of CdTe units have been investigated for lowest energy geometry and stability.^{19–22} As the number of atoms increases in Cd_nTe_n clusters, the predicted structures change from simple planar structures to more complicated three-dimensional structures and multiple structures can be predicted for clusters with the same number of CdTe units. Hollow cages and endohedral or core–shell cage structures for a single Cd_nTe_n cluster have been reported.²³ Magic size quantum dots such as Cd₃₃Se₃₃ and Cd₃₃Te₃₃ have been simulated to evaluate their structural and electronic properties both in the bare form and when capped with ligands.²⁴ The structural and electronic properties of small-sized nanoparticles ($n = 6, 9$) of CdSe and CdTe have also been computed for both the bare and capped forms.²⁵ A comparative study (DFT) of seven telluride compounds, such as XTe (X = Bi, Cd, Pb, Zn), X₂Te₃ (X = Bi, Sb) and X₂Y_xTe_{3-x} (X = Bi, Y = Se, x = 0 to 0.3) revealed CdTe to be the best compound for conductivity as compared to other compounds.²⁶ A theoretical investigation of CdTe multi-cage nanochains demonstrated their increased stability and factors such as the assembly mode and the number of cages were shown to affect the energy gap, density of states and charge density distribution.²⁷

The aim of the present study is to explore possible structures for Cd_nTe_n with optimized geometries and the lowest energy for each cluster. We performed DFT calculations to systematically optimize the most stable geometries and explore the electronic properties of Cd_nTe_n ($n = 1$ –17) clusters. Band gap analysis of these clusters has also been performed and is discussed in detail.

2 Computational methods

Initial structural geometries were obtained from the published literature, an unbiased search on the potential energy surface

was performed using a stepwise simulated annealing technique incorporating first-principles molecular dynamics.^{19–21,23} Furthermore, we employed the particle swarm optimization (PSO)^{28,29} technique as implemented in CALYPSO^{30,31} using PWSCF code³² as the DFT engine to expand the canvas of candidate structures. For the CALYPSO structural search, we set different parameters for the population size and the number of generations for the PSO algorithm. The population size and the number of generations was fixed to 10 for Cd_nTe_n ($n = 1$ –5), 20 for Cd_nTe_n ($n = 6$ –9) and 30 for Cd_nTe_n ($n = 10$ –17). Many candidate geometries were also constructed manually considering the hexagonal and wurtzite crystal motifs for Cd_nTe_n clusters. Some of the initial structures were adopted from published studies on semiconductor clusters such as GaAs, GaN, BN, and ZnO. After initial screening, the most probable candidate geometries with the lowest energies were first optimized using hybrid functional B3LYP³³ with basis sets of Los Alamos double- ζ effective core potential (Lanl2dz)^{34–36} and were then optimized again using a PBE0 (ref. 37) hybrid functional with basis sets of Los Alamos double- ζ effective core potential (Lanl2dz). The PBE0 functional has been previously found to provide a good description of the semiconductor clusters.^{38,39} In order to accommodate the dispersions, empirical dispersion parameters (PBE0-D3) were implemented as proposed by Grimme *et al.*⁴⁰ All of the calculations for the candidate structures and final structures were carried out using both the B3LYP/Lanl2dz and PBE0-D3/Lanl2dz approaches and implemented in the Gaussian 09W software package.⁴¹ Only the lowest energy structure of each Cd_nTe_n cluster ($n = 1$ –9) was considered suitable to study the electronic properties. Two types of isomeric structures (*i.e.*, hollow cages and endohedral or core–shell cages structures) were constructed for the larger clusters Cd_nTe_n ($n = 10$ –17). All of the calculations were performed in the gas phase. Frequency analysis was performed at the same DFT theory levels to insure that the optimized structures were the true minima and not transition states (confirmed by the absence of an imaginary frequency). Single point second-order Møller–Plesset perturbation theory (MP2)^{42–44} energy calculations were performed using a larger basis set Def2-TZVP⁴⁵ to evaluate the energy values of the final lowest energy structure and were found to be in better agreement with the PBE0-D3/Lanl2dz calculations than with the B3LYP/Lanl2dz calculations. Therefore, the results of the PBE0-D3/Lanl2dz calculations are discussed throughout this paper unless mentioned otherwise, and the results of the B3LYP/Lanl2dz and MP2/Def2-TZVP approaches are given in Tables S1 and S2 (ESI†), respectively.

The binding energies, highest occupied molecular orbital (HOMO)/lowest unoccupied molecular orbital (LUMO) band gaps, dipole moments and static dipole polarizabilities were also calculated. The calculated structures and molecular orbitals of the Cd_nTe_n clusters were visualized using GaussView software.

3 Results and discussion

Before discussing the results of the present study, two previous reports published by Bhattacharya²⁰ and Zhao²¹ are worth mentioning. Both reports describe the theoretical investigation



of Cd_nTe_n clusters. These previously published reports are based on plane-wave DFT methods. The plane-wave DFT method expands the Kohn-Sham orbitals in terms of the plane waves, up to a certain maximum kinetic energy and assumes the system to be fully periodic. However, the present work is based on the localized-orbital (Gaussian) DFT approach. Therefore, comparison of the results must be performed while keeping the different nature of the DFT approaches in mind. The optimized geometries of the Cd_nTe_n clusters are presented in Fig. 1 and 2. Fig. 1 shows the gas phase optimized hollow cage type structures of Cd_nTe_n , in which $n = 1-9$. Fig. 2 shows the structures of the two types; hollow cage and core-shell cage geometries. Zhao *et al.* reported that the core-shell cage structures were more stable than the hollow cages for $n \geq 12$.²¹ However, our calculations revealed that the core-shell cage structures become more stable than the hollow cages for $n \geq 9$.

The calculated binding energies of all of the optimized configurations studied in this work are given in Table 1. The binding energy (E_b) per Cd-Te unit was calculated for the optimized geometries using the following expression:

$$E_b = \{n[E(\text{Cd}) + E(\text{Te})] - E(\text{Cd}_n\text{Te}_n)\}/n$$

In which $E(\text{A})$ indicates the total energy of system A.

CdTe is optimized as a dimer and a bond length of 2.61 Å and 2.65 Å at the PBE0-D3/Lanl2dz and B3LYP/Lanl2dz levels of theories was observed, respectively. Previous calculations by Zhao and co-workers²¹ predicted a bond length of 2.61 Å and Bhattacharya and Kshirsagar¹⁸ predicted a bond length of 2.57 Å.

For the Cd_nTe_n clusters in which $2 \leq n \leq 8$, Cd and Te atoms adapt to alternate positions with a planar geometry and a coordination number of two. The optimized structure of Cd_2Te_2 is a rhombus (D_{2h}), and for Cd_3Te_3 is planar (C_{3h}) with Cd-Te bond lengths of 2.79 Å and 2.73 Å at the PBE0-D3/Lanl2dz level of theory, respectively, which agrees with the bond length predicted by Zhao and co-workers,²¹ while Cd_2Te_2 and Cd_3Te_3 showed bond lengths of 2.83 Å and 2.77 Å at the B3LYP/Lanl2dz levels of theory, respectively. This comparison of bond lengths revealed a difference of 0.04 Å when the clusters are optimized with the PBE0-D3/Lanl2dz and B3LYP/Lanl2dz levels of theories. Two different geometries (T_d and D_{4h}) for Cd_4Te_4 were found. These two geometries were found to be very close in terms of energy with an energy difference of 0.49 eV making the tetrahedral (T_d) geometry a little more stable as compared to the square planar (D_{4h}) structure. This finding is different from that found in the study published by Zhao and co-workers who reported that the square planar geometry had the minimum energy. The Cd-Te bond lengths for the tetrahedral Cd_4Te_4 and square Cd_4Te_4 were calculated to be 2.95 Å and 2.75 Å, respectively. Cd_5Te_5 adapts a non-symmetric 3D distorted envelop structure and has a Cd-Te bond length of 2.71 Å, unlike the planar pentagon structure reported by Bhattacharya and Zhao. A planar to 3D shift starts to occur at $n = 5$ as we observe a distortion from the planar geometry.

The lowest-energy structures of Cd_nTe_n with $n = 6-9$ are closed polyhedral cages, which is in agreement with the previous reports. These structures are mainly composed of 4-membered and 6-membered rings with an alternate Cd and Te

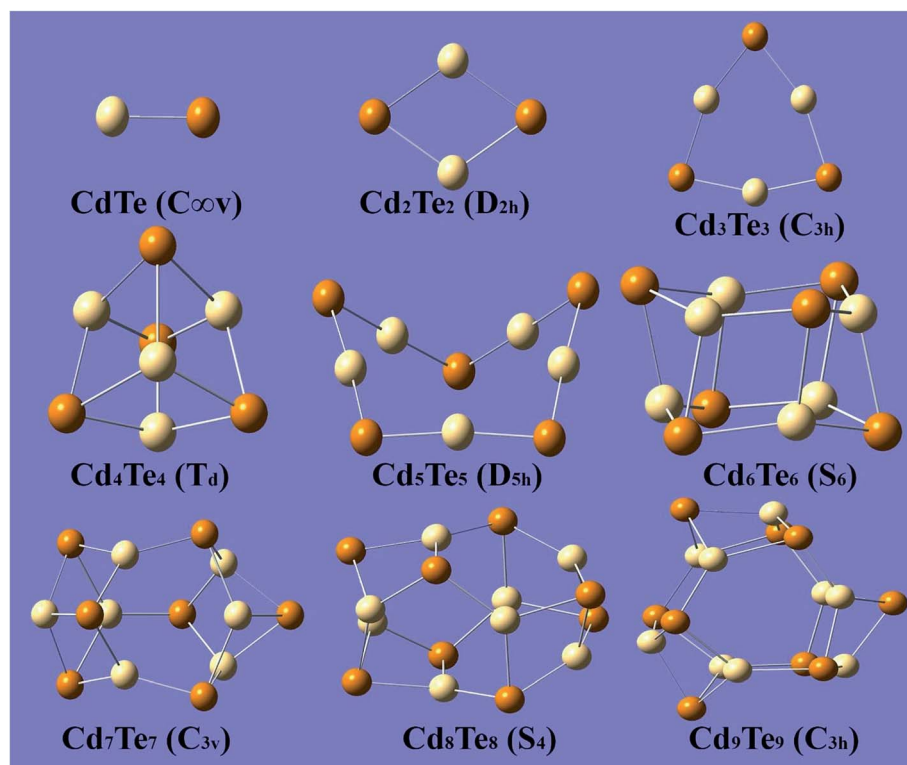


Fig. 1 The lowest-energy optimized structures of Cd_nTe_n ($n = 1-9$) with the point group symmetry. Te is indicated with dark colored spheres and Cd with light colored spheres.



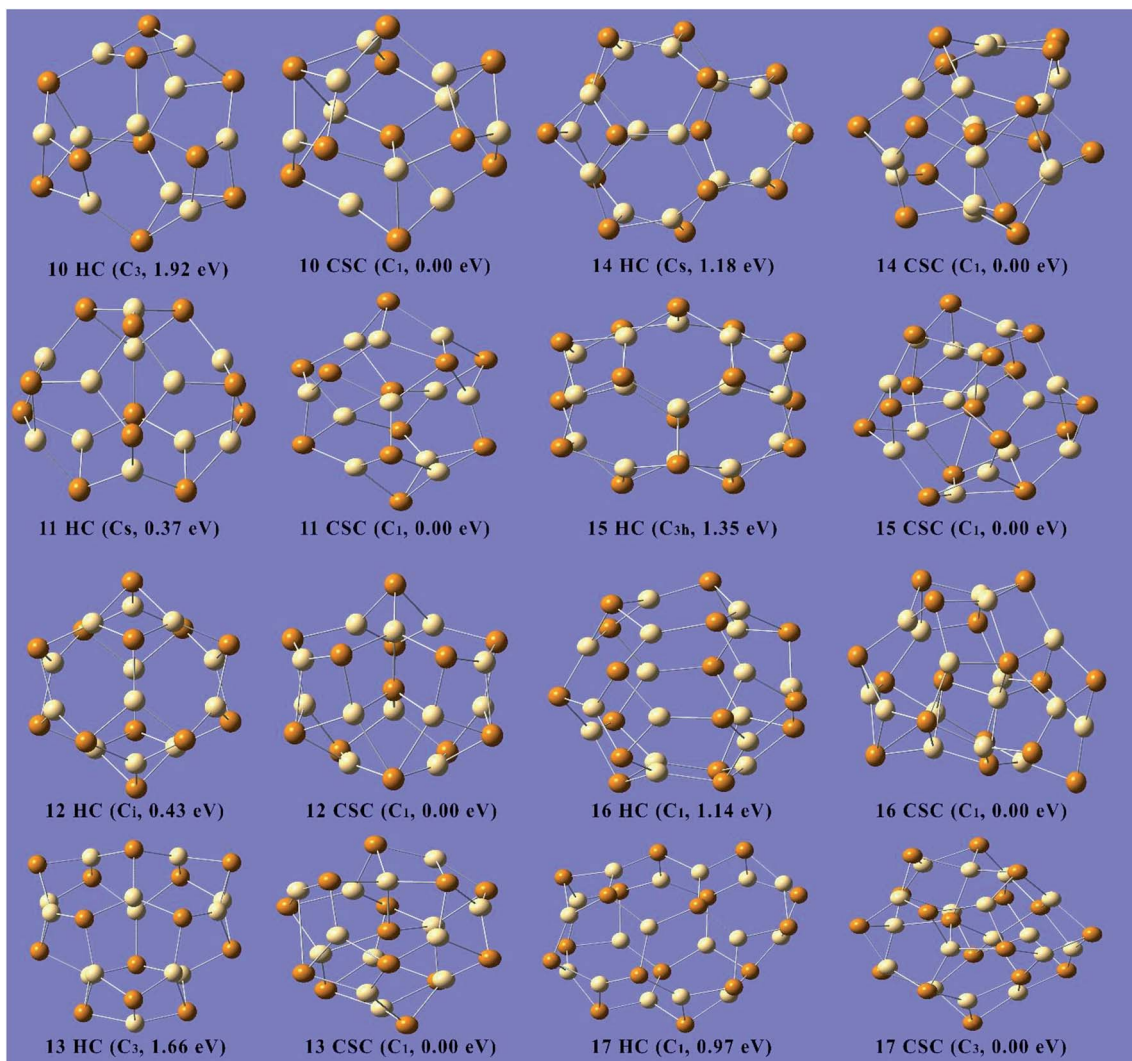


Fig. 2 The lowest-energy optimized structure of Cd_nTe_n ($n = 10-17$), both isomers, that is, the hollow cage (HC) structures and the core–shell cage (CSC) structures are given with the point group symmetry and the ground state energy difference of the two isomeric structures. Dark colored spheres indicate Te and light colored spheres indicate Cd atoms.

atomic arrangement. For these polyhedral cages, the coordination number increases from two to three. For $n = 6$, the minimum energy structure has a S_6 point group. The optimized structure is composed of two six-membered rings. For Cd_7Te_7 , the optimized structure consists of three six-membered rings and six four-membered rings that have C_{3v} symmetry. This optimized geometry agrees with the previously reported structure for Cd_7Te_7 . The optimized geometry of Cd_8Te_8 consists of four distorted 6-membered rings and six 4-membered rings and has a S_4 point group. The lowest-energy structure of Cd_9Te_9 consists of five distorted 6-membered rings and six 4-membered rings with a C_{3h} point group.

Two classes of the most stable structures were elucidated for the clusters with $n = 10-17$. These structures are categorized into the hollow cage structures with an empty center and the endohedral or core–shell cage structures with one or more atoms inside the cage. The structures for lowest energy of clusters $n = 10-17$ of both classes are shown in Fig. 2. All of the

core–shell structures contain at least one atom at the center of the cage, whereas the hollow cage structures have an empty center. The lowest-energy hollow cage structure for $\text{Cd}_{10}\text{Te}_{10}$ has a C_3 point group symmetry and is composed of six six-membered rings and six four-membered rings, while the core–shell structure for the $\text{Cd}_{10}\text{Te}_{10}$ cluster has a point group of C_1 and has a 1.92 eV lower energy than the hollow cage structure, and is hence more stable than the hollow cage structure (as shown in Fig. 2). The idea of the core–shell structure comes from the previously published work by Zhao *et al.*²¹ in which they employed first-principles molecular dynamics algorithms to search for the possible geometries. Herein, the favorable presence of the core–shell Cd_nTe_n ($n \geq 10$) clusters was predicted using the localized-orbitals DFT approach.

Similarly, the core–shell structures of the clusters $\text{Cd}_{11}\text{Te}_{11}$ and $\text{Cd}_{12}\text{Te}_{12}$ both have C_1 point group symmetry as compared to the hollow cage structures that have C_s and C_i point group symmetries, respectively. Both of the core–shell structures were



Table 1 The relative energy (E_e , the energy of the putative global minimum is referenced to zero), binding energy (E_b) in eV per CdTe unit, HOMO and LUMO energies, dipole moments (μ) and polarizability per CdTe unit ($\langle\alpha\rangle$) for the lowest energy optimized structures of Cd_nTe_n ($n = 1-17$), the hollow cage and the endohedral (core–shell) cage structures ($n = 10-17$)

Cluster	E_b (eV per unit)	HOMO/LUMO (eV)	μ (debye)	$\langle\alpha\rangle$ (bohr ³ per unit)
Cd_1Te_1	2.01	−5.7/−4.07	5.8233	78.59
Cd_2Te_2	3.76	−5.83/−3.21	0	71.49
Cd_3Te_3	4.45	−6.31/−2.67	0.0001	72.71
Cd_4Te_4	4.68	−6.44/−2.98	0.0003	70.01
Cd_5Te_5	4.56	−6.15/−2.86	0.6762	78.88
Cd_6Te_6	5	−6.38/−2.81	0.0001	70.62
Cd_7Te_7	5.01	−6.41/−2.76	1.2246	71.4
Cd_8Te_8	5.11	−6.41/−2.76	0.0001	71.43
Cd_9Te_9	5.16	−6.53/−2.78	0.0022	71.14

Core–shell cages					Hollow cages					
E_e (eV)	E_b (eV per unit)	HOMO/LUMO (eV)	μ (debye)	$\langle\alpha\rangle$ (bohr ³ per unit)	E_e (eV)	E_b (eV per unit)	HOMO/LUMO (eV)	μ (debye)	$\langle\alpha\rangle$ (bohr ³ per unit)	
$\text{Cd}_{10}\text{Te}_{10}$	0.00	5.2	−6.19/−2.81	3.198	71.05	1.92	4.97	−6.4/−2.83	1.4702	71.81
$\text{Cd}_{11}\text{Te}_{11}$	0.00	5.2	−6.32/−2.95	4.2208	71.11	0.37	5.21	−6.46/−2.8	1.2824	71.95
$\text{Cd}_{12}\text{Te}_{12}$	0.00	5.3	−6.36/−2.92	1.5299	69.84	0.43	5.25	−6.76/−2.76	0.0018	71.77
$\text{Cd}_{13}\text{Te}_{13}$	0.00	5.4	−6.47/−2.79	3.4536	70.1	1.66	5.25	−6.44/−2.87	1.9381	73.53
$\text{Cd}_{14}\text{Te}_{14}$	0.00	5.3	−6.04/−3.02	2.3672	71.89	1.18	5.25	−6.52/−2.87	0.8573	72.78
$\text{Cd}_{15}\text{Te}_{15}$	0.00	5.4	−6.37/−3.2	5.4224	72.03	1.35	5.27	−6.66/−2.86	0.0007	72.7
$\text{Cd}_{16}\text{Te}_{16}$	0.00	5.3	−5.81/−2.97	5.683	72.63	1.14	5.27	−6.61/−2.91	0.4124	72.79
$\text{Cd}_{17}\text{Te}_{17}$	0.00	5.4	−6.27/−2.99	10.788	71.71	0.97	5.31	−6.51/−2.95	3.4917	73.62

found to be more stable than their counterpart hollow cage structures by 0.37 and 0.43 eV, respectively. The cluster $\text{Cd}_{13}\text{Te}_{13}$ was an exception and its core–shell structure is more stable than all of the others studied structures with a binding energy of 5.38 eV per unit. The most stable hollow cage structure for the $\text{Cd}_{13}\text{Te}_{13}$ cluster contains nine six-membered rings and six four-membered rings in its cage with a C_3 point group symmetry, while the core–shell structure has a C_1 point group and has 1.66 eV lower energy than the hollow cage structure. The most stable hollow cage structure for the $\text{Cd}_{14}\text{Te}_{14}$ cluster is composed of ten six-membered rings, and six four-membered rings with point group C_s symmetry, whereas the core–shell structure of the $\text{Cd}_{14}\text{Te}_{14}$ cluster has a C_1 point group and has a 1.18 eV lower energy than the hollow cage structure, and is hence more stable. The hollow cage structure of $\text{Cd}_{15}\text{Te}_{15}$ is made of six four-membered rings and eleven six-membered rings with a C_{3h} point group symmetry and is less stable than the core–shell structure of $\text{Cd}_{15}\text{Te}_{15}$ (C_1 point group symmetry) by 1.35 eV. The core–shell structure $\text{Cd}_{16}\text{Te}_{16}$ contains two (one Cd and one Te atom) atoms inside the cage with a C_1 point group and is found to be more stable than a hollow cage of the $\text{Cd}_{16}\text{Te}_{16}$ cluster, which is composed of six-four membered rings and twelve six-membered rings (C_1 point group symmetry), by 1.14 eV. The hollow cage of the $\text{Cd}_{17}\text{Te}_{17}$ cluster has thirteen six-membered rings and six four-membered rings with a C_1 point group symmetry, while the core–shell structure of this cluster (C_3 point group) is more stable than its hollow cage counterpart by 0.97 eV. From the above discussion, it can be generalized that out of these two configurations the core–

shell cage configurations are the most stable as compared to the hollow cage configurations for all of the cluster sizes.

The binding energies of the clusters calculated using the PBE0-D3/Lanl2dz level of theory (as shown in Table 1) are somewhat different from the calculations with the B3LYP/Lanl2dz level of theory (see Table S1, ESI†). The inclusion of dispersion interactions in the theoretical simulations is considered advantageous to achieving chemical accuracy.^{40,46}

In order to understand the electronic properties of the Cd_nTe_n clusters, the HOMO–LUMO energy gaps were calculated (see Fig. 3 and 4). We understand that the HOMO–LUMO energy gap values should be used with caution, but we have used them to show how the electronic properties of the clusters studied change along with the cluster size and geometries. The HOMO–LUMO gap analysis did not reveal a regular trend based on the size and geometries of the Cd_nTe_n clusters, except that noticeably higher HOMO–LUMO gaps were observed for the hollow cage isomers as compared to the core–shell structures (see Fig. 4). The CdTe dimer had the smallest HOMO–LUMO gap of 1.63 eV. The HOMO–LUMO gaps of all of the other clusters varied between 2.62 eV (HOMO–LUMO gap of Cd_2Te_2 structure) and 4.00 eV (HOMO–LUMO gap of $\text{Cd}_{12}\text{Te}_{12}$ hollow cage structure) and no systematic change in the gap energy was observed in these nanoclusters. The $\text{Cd}_{12}\text{Te}_{12}$ hollow cage structure demonstrated the highest HOMO–LUMO gap (4.00 eV) amongst all of the clusters. Interestingly, the Cd_9Te_9 cluster has a HOMO–LUMO gap of 3.75 eV, which is the largest HOMO–LUMO gap amongst the small Cd_nTe_n clusters ($n = 1-9$, Fig. 3).



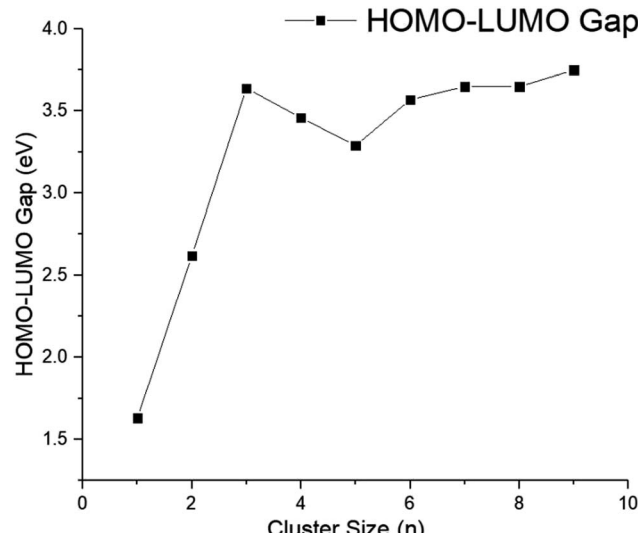


Fig. 3 HOMO–LUMO gaps for the Cd_nTe_n nanocluster ($n = 1\text{--}9$).

The dipole moments for the lowest-energy structures of all of the types of clusters were computed to understand the symmetries of the structures (dipole moments for all of the structures are presented in Table 1). Most of the small size clusters Cd_nTe_n ($n = 2\text{--}9$) show minimal values for the dipole moments (close to zero) owing to the highly ordered and symmetric configurations of these structures. As the CdTe dimer is a linear structure, it possesses a very high dipole moment (5.8233 debye). Another exception is observed for the Cd_5Te_5 cluster with a C_1 symmetry and the Cd_7Te_7 cluster with a C_{3v} symmetry which have a relatively high dipole moment (0.6762 and 1.2246 debye, respectively) as compared to the other small size clusters ($n = 2\text{--}9$). For the isomers of the larger clusters ($n = 10\text{--}17$), it was observed that the core–shell structures have higher values for the dipole moments than the hollow cage structures because of the highly symmetric structures of the hollow cages of Cd_nTe_n ($n = 10\text{--}17$) with the symmetries: C_3 , C_s , C_i , and C_{3h} . The hollow cage structures have a symmetric charge distribution around the geometric centers, and hence small dipole moments, while the core–shell structures are nonsymmetrical and therefore have high values for the dipole moments.

The mean polarizability per CdTe unit is presented in Table 1 and Fig. 5. The isotropic polarizability is an average of the polarizability in all orientations taken as a function of the cluster size. Therefore, the mean polarizability per CdTe unit can be defined as:

$$\langle \alpha \rangle = \frac{1}{3n} (\alpha_{xx} + \alpha_{yy} + \alpha_{zz})$$

Fig. 5 shows a trend for the polarizability in relation to the size and geometry of the Cd_nTe_n clusters. Cd_5Te_5 showed the highest value for the mean polarizability $\langle \alpha \rangle$ owing to its distorted out of plane envelop geometry. It is evident that all the core–shell cage structures exhibited lower polarizabilities than the respective hollow cage structures. The core–shell $\text{Cd}_{12}\text{Te}_{12}$

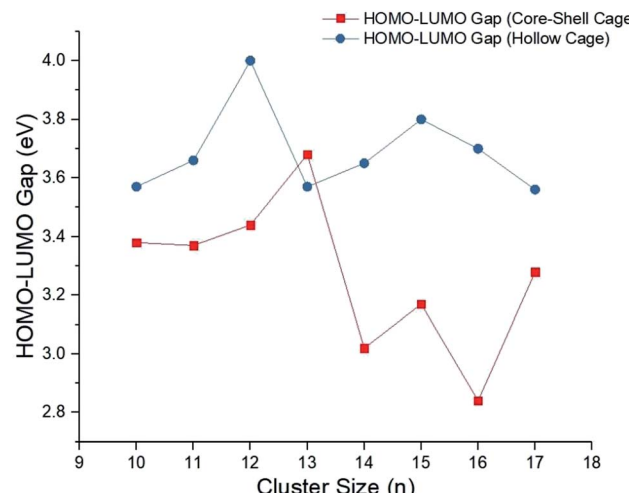


Fig. 4 HOMO–LUMO gaps for the Cd_nTe_n nanoclusters of both the isomeric structure core–shell cages and the hollow cages ($n = 10\text{--}17$).

has the lowest value of mean polarizability $\langle \alpha \rangle$ (69.84 bohr³ per unit) compared to all of the other clusters. These results revealed that the geometries of the clusters greatly influence the polarizability, and changes in the geometries from planer to three dimensional and open geometries to more compact geometries lower the value of polarizability.⁴⁷

Fig. 6 shows the plots of the HOMO and LUMO of the representative clusters and plots of the HOMO and LUMO of all of the studied clusters are presented in the ESI (Fig. S1 and S2†). The electron densities of the HOMOs lie on the surface of the cage for the hollow cage structures while in the case of the core–shell structures the electrons densities of the HOMO are distributed both on the surface and the interior of the structures. This HOMO and LUMO analysis also revealed a trend for the electron densities localization in the HOMO of the clusters, while a clear delocalization of electron densities is demonstrated by the LUMO of the clusters. This electron density

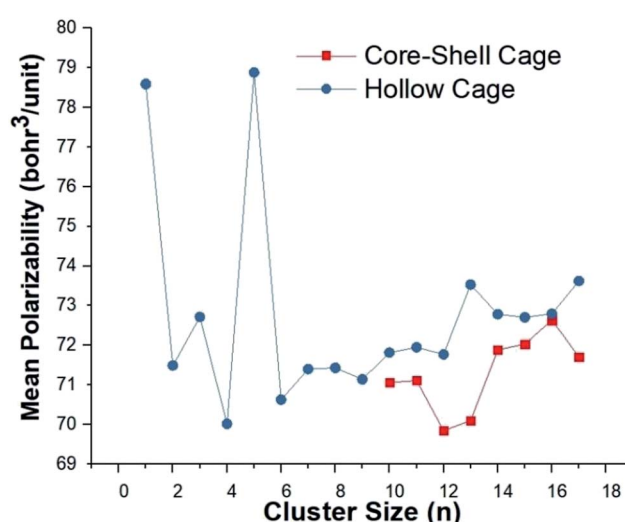


Fig. 5 Mean polarizability (bohr³ per unit) for the two isomeric forms of the Cd_nTe_n nanoclusters.



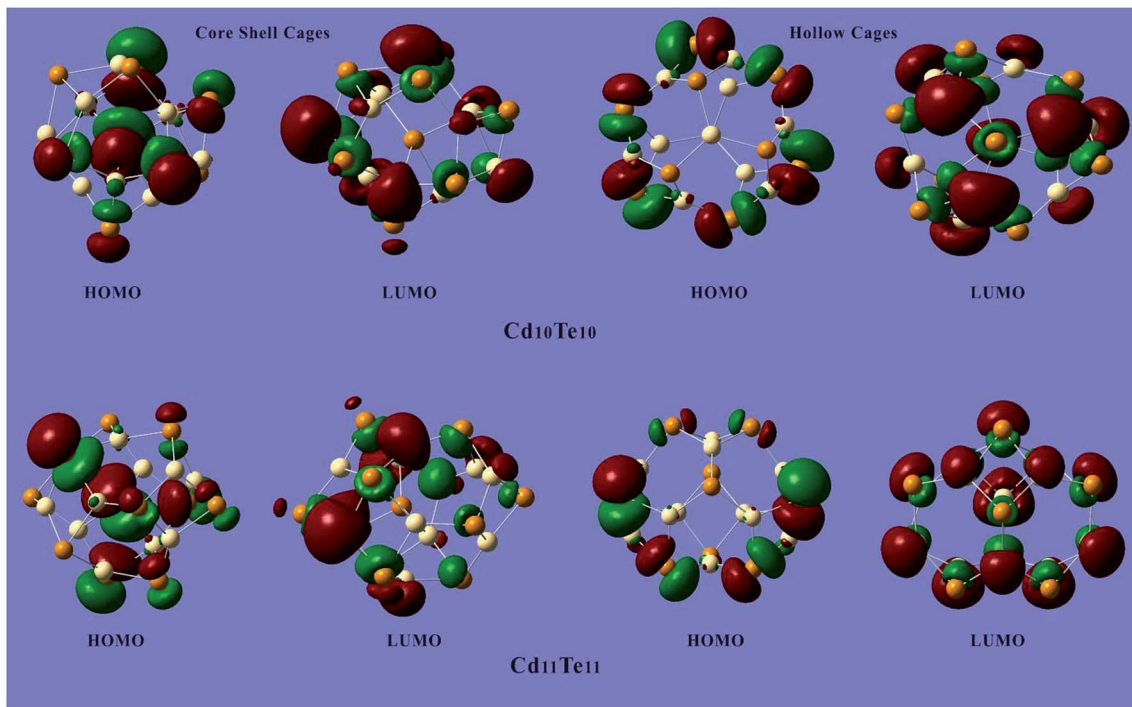


Fig. 6 The HOMO and LUMO representative of the most stable lowest-energy clusters of Cd_nTe_n .

delocalization is also quite pronounced for the LUMO+1, and LUMO+2 of the clusters studied (see ESI†).

4 Conclusions

As the number of atoms increases in the Cd_nTe_n clusters, the predicted structures change from simple planar structures to more complicated 3D-structures. Multiple structures can be predicted for clusters with the same number of CdTe units. The hollow cage and the endohedral or core-shell cage structures for the same Cd_nTe_n clusters have been reported previously. We have performed systematic DFT and MP2 studies to evaluate the structures and electronic properties of the Cd_nTe_n ($n = 1-17$) clusters. The study results can be summarized as follows:

(i) For the Cd_nTe_n clusters with $2 \leq n \leq 8$, the Cd and Te atoms adapt alternate positions with a planar geometry and a coordination number of two. Two different geometries (T_d and D_{4h}) were found for Cd_4Te_4 . These geometries were found to be very close in energy, with an energy difference of only 0.12 eV, making the tetrahedral structure a little more stable. The Cd_5Te_5 cluster was shown to adopt a non-symmetric 3D distorted envelop structure, unlike the planar pentagon structure reported by Bhattacharya and Zhao. Thus, a planar-to-3D shift starts to occur at $n = 5$ as we observe distortion from the planar geometry.

(ii) The lowest-energy structures for Cd_nTe_n with $n = 6-9$ were found to be closed polyhedral cages, in agreement with the previous reports. These structures are mainly composed of 4-membered and 6-membered rings with an alternate Cd and Te atomic arrangement. For these polyhedral cages, the coordination number increases from two to three.

(iii) Two classes of the most stable structures were elucidated for the clusters with $n = 10-17$. These structures were categorized into the hollow cage structure with an empty center and the endohedral or core-shell cage structure with one or more atoms inside the cage. All the core-shell structures were shown to contain at least one atom at the center of the cage. The idea of the core-shell structure comes from the previously published work by Zhao *et al.*²¹ in which the researchers employed first-principles MD algorithms to search for the possible geometries. In our study, the favorable presence of the core-shell Cd_nTe_n ($n \geq 9$) clusters was predicted using the localized-orbitals DFT approach.

(iv) The most stable species, according to their binding energy values, eV per unit, were calculated to be the $\text{Cd}_{12}\text{Te}_{12}$ (core-shell cage) 5.29 eV per unit, $\text{Cd}_{13}\text{Te}_{13}$ (core-shell cage) 5.38 eV per unit, $\text{Cd}_{14}\text{Te}_{14}$ (core-shell cage) 5.33 eV per unit, $\text{Cd}_{15}\text{Te}_{15}$ (core-shell cage) 5.36 eV per unit, $\text{Cd}_{16}\text{Te}_{16}$ (core-shell cage) 5.34 eV per unit, $\text{Cd}_{17}\text{Te}_{17}$ (core-shell cage) 5.37 eV per unit, and the $\text{Cd}_{17}\text{Te}_{17}$ (hollow cage) 5.31 eV per unit. The binding energies were found to increase significantly up to $n = 9$ and then varied within a 0.19 eV range (see Table 1).

(v) The HOMO-LUMO gap analysis revealed no regular trend based on the size and geometries of the Cd_nTe_n clusters, except that noticeably higher HOMO-LUMO gaps were observed for the hollow cage isomers as compared to the core-shell structures. The CdTe dimer has the smallest HOMO-LUMO gap of 1.63 eV. The HOMO-LUMO gaps of all of the other clusters vary between 2.62 eV (HOMO-LUMO gap of Cd_2Te_2) and 4.0 eV (HOMO-LUMO gap of the $\text{Cd}_{12}\text{Te}_{12}$ hollow cage structure). The $\text{Cd}_{12}\text{Te}_{12}$ hollow cage structure demonstrated the highest HOMO-LUMO gap (4.0 eV) amongst all of the clusters.



(vi) For the larger clusters with $n = 10\text{--}12$ the HOMO-LUMO gap values increase gradually and $\text{Cd}_{12}\text{Te}_{12}$ (hollow cage) showed the highest value, with a HOMO-LUMO gap of 4.00 eV. For clusters with $n = 13\text{--}17$ the HOMO-LUMO gap values vary randomly with a sudden increase and sharp decrease, the $\text{Cd}_{16}\text{Te}_{16}$ (core-shell cage) has a HOMO-LUMO gap value of 2.84 eV which is the lowest amongst the larger clusters. The $\text{Cd}_{15}\text{Te}_{15}$ (hollow cage), cluster has the second largest HOMO-LUMO gap, 3.80 eV amongst the investigated clusters. Among the small Cd_nTe_n clusters ($n = 1\text{--}9$) the largest HOMO-LUMO gap 3.75 eV was shown by the Cd_9Te_9 cluster. In general, for the hollow cage isomers, the HOMO-LUMO gap changes are much less pronounced than for the core-shell structures.

(vii) The core-shell cage structures exhibited lower polarizabilities than the respective hollow cage structure. The core-shell $\text{Cd}_{12}\text{Te}_{12}$ has the lowest value for the mean polarizability $\langle\alpha\rangle$ (69.84 bohr³ per unit) than all of the other clusters. These results revealed that the geometries of the clusters greatly influence the polarizability, and that changes in the geometries from planar to three dimensional and open to more compact geometries lower the value of the polarizability.

We propose that our findings contribute a more profound and detailed understanding of the trends in the changes in the structural and electronic properties of the Cd_nTe_n nanoclusters and will be helpful in both computational and experimental studies of larger CdTe NP-containing systems.

Conflicts of interest

There are no conflicts to declare.

References

- 1 S. V. Kershaw, L. Jing, X. Huang, M. Gao and A. L. Rogach, *Mater. Horiz.*, 2017, **4**, 155–205.
- 2 H. Zou, M. Liu, D. Zhou, X. Zhang, Y. Liu, B. Yang and H. Zhang, *J. Phys. Chem. C*, 2017, **121**, 5313–5323.
- 3 M. Amelia, C. Lincheneau, S. Silvi and A. Credi, *Chem. Soc. Rev.*, 2012, **41**, 5728–5743.
- 4 C. C. Tu and L. Y. Lin, *Appl. Phys. Lett.*, 2008, **93**, 6–9.
- 5 D. A. R. Barkhouse, A. G. Pattantyus-Abraham, L. Levina and E. H. Sargent, *ACS Nano*, 2008, **2**, 2356–2362.
- 6 N. Yaacobi-Gross, N. Garphunkin, O. Solomeshch, A. Vaneski, A. S. Susha, A. L. Rogach and N. Tessler, *ACS Nano*, 2012, **6**, 3128–3133.
- 7 J. W. Xiao, S. Ma, S. Yu, C. Zhou, P. Liu, Y. Chen, H. Zhou and Y. Li, *Nano Energy*, 2018, **46**, 45–53.
- 8 J. Huang, B. Xu, C. Yuan, H. Chen, J. Sun, L. Sun and H. Agren, *ACS Appl. Mater. Interfaces*, 2014, **6**, 18808–18815.
- 9 G. H. Carey, A. L. Abdelhady, Z. Ning, S. M. Thon, O. M. Bakr and E. H. Sargent, *Chem. Rev.*, 2015, **115**, 12732–12763.
- 10 A. Bosio, G. Rosa and N. Romeo, *Sol. Energy*, 2018, **175**, 31–43.
- 11 P. O. Anikeena, J. E. Halpert, M. G. Bawendi and V. Bulovic, *Nano Lett.*, 2009, **9**, 2532–2536.
- 12 S. Kanagasubbulakshmi, R. Kathiresan and K. Kadirvelu, *Colloids Surf., A*, 2018, **549**, 155–163.
- 13 H. Liang, D. Song and J. Gong, *Biosens. Bioelectron.*, 2014, **53**, 363–369.
- 14 V. I. Klimov, *Nanocrystal quantum dots*, 2010.
- 15 S. V. Kilina, P. K. Tamukong and D. S. Kilin, *Acc. Chem. Res.*, 2016, **49**, 2127–2135.
- 16 B. Rajbanshi, S. Sarkar and P. Sarkar, *J. Mater. Chem. C*, 2014, **2**, 8967–8975.
- 17 S. Sarkar, S. Saha, S. Pal and P. Sarkar, *RSC Adv.*, 2014, **4**, 14673–14683.
- 18 S. K. Bhattacharya and A. Kshirsagar, *Eur. Phys. J. D*, 2008, **48**, 355–364.
- 19 P. Seal, S. Sen and S. Chakrabarti, *Chem. Phys.*, 2010, **367**, 152–159.
- 20 S. K. Bhattacharya and A. Kshirsagar, *Phys. Rev. B*, 2007, **75**, 035402.
- 21 J. Wang, L. Ma, J. Zhao and K. A. Jackson, *J. Chem. Phys.*, 2009, **130**, 214307.
- 22 P. Karamanis and C. Pouchan, *Chem. Phys. Lett.*, 2009, **474**, 162–167.
- 23 L. Ma, J. Wang and G. Wang, *Chem. Phys. Lett.*, 2012, **552**, 73–77.
- 24 A. E. Kuznetsov and D. N. Beratan, *J. Phys. Chem. C*, 2014, **118**, 7094–7109.
- 25 E. Lim, A. E. Kuznetsov and D. N. Beratan, *Chem. Phys.*, 2012, **407**, 97–109.
- 26 E. V. Shah and D. R. Roy, *Comput. Mater. Sci.*, 2014, **88**, 156–162.
- 27 Z. Wu, Y. Zhang, S. Huang and S. Zhang, *Comput. Mater. Sci.*, 2013, **68**, 238–244.
- 28 R. C. Eberhart and Y. Shi, *Proc. Congress on Evolutionary Computation*, 2001.
- 29 R. C. Eberhart and J. Kennedy, *Proceedings of the Sixth International Symposium on Micro Machine and Human Science*, 1995, pp. 39–43.
- 30 Y. Wang, J. Lv, L. Zhu and Y. Ma, *Phys. Rev. B*, 2010, **82**, 094116.
- 31 Y. Wang, J. Lv, L. Zhu and Y. Ma, *Comput. Phys. Commun.*, 2012, **183**, 2063–2070.
- 32 P. Giannozzi, S. Baroni, N. Bonini, M. Calandra, R. Car, C. Cavazzoni, D. Ceresoli, G. L. Chiarotti, M. Cococcioni, I. Dabo and A. Dal Corso, *J. Phys.: Condens. Matter*, 2009, **21**, 395502.
- 33 A. D. Becke, *J. Chem. Phys.*, 1993, **98**, 5648–5652.
- 34 P. J. Hay and W. R. Wadt, *J. Chem. Phys.*, 1985, **82**, 270–283.
- 35 W. R. Wadt and P. J. Hay, *J. Chem. Phys.*, 1985, **82**, 284–298.
- 36 P. J. Hay and W. R. Wadt, *J. Chem. Phys.*, 1985, **82**, 299–310.
- 37 C. Adamo and V. Barone, *J. Chem. Phys.*, 1999, **110**, 6158–6170.
- 38 K. A. Nguyen, R. Pachter, P. N. Day and H. Su, *J. Chem. Phys.*, 2015, **142**, 234305.
- 39 K. A. Nguyen, R. Pachter, J. Jiang and P. N. Day, *J. Phys. Chem. A*, 2018, **122**, 6704–6712.
- 40 S. Grimme, J. Antony, S. Ehrlich and H. Krieg, *J. Chem. Phys.*, 2010, **132**, 154104.
- 41 M. J. Frisch, G. W. Trucks, H. B. Schlegel, G. E. Scuseria, M. A. Robb, J. R. Cheeseman, G. Scalmani, V. Barone, B. Mennucci, G. A. Petersson, H. Nakatsuji, M. Caricato,

X. Li, H. P. Hratchian, A. F. Izmaylov, J. Bloino, G. Zheng, J. L. Sonnenberg, M. Hada, M. Ehara, K. Toyota, R. Fukuda, J. Hasegawa, M. Ishida, T. Nakajima, Y. Honda, O. Kitao, H. Nakai, T. Vreven, J. A. Montgomery Jr, J. E. Peralta, F. Ogliaro, M. Bearpark, J. J. Heyd, E. Brothers, K. N. Kudin, V. N. Staroverov, R. Kobayashi, J. Normand, K. Raghavachari, A. Rendell, J. C. Burant, S. S. Iyengar, J. Tomasi, M. Cossi, N. Rega, J. M. Millam, M. Klene, J. E. Knox, J. B. Cross, V. Bakken, C. Adamo, J. Jaramillo, R. Gomperts, R. E. Stratmann, O. Yazyev, A. J. Austin, R. Cammi, C. Pomelli, J. W. Ochterski, R. L. Martin, K. Morokuma, V. G. Zakrzewski, G. A. Voth, P. Salvador, J. J. Dannenberg, S. Dapprich, A. D. Daniels, O. Farkas, J. B. Foresman, J. V. Ortiz, J. Cioslowski, and D. J. Fox, *Gaussian 09, Revision A.1*, Gaussian, Inc., Wallingford CT, 2009.

42 M. J. Frisch, M. Head-Gordon and J. A. Pople, *Chem. Phys. Lett.*, 1990, **166**, 275–280.

43 M. J. Frisch, M. Head-Gordon and J. A. Pople, *Chem. Phys. Lett.*, 1990, **166**, 281–289.

44 M. Head-Gordon, J. A. Pople and M. J. Frisch, *Chem. Phys. Lett.*, 1988, **153**, 503–506.

45 F. Weigend and R. Ahlrichs, *Phys. Chem. Chem. Phys.*, 2005, **7**, 3297–3305.

46 S. Grimme, *Wiley Interdiscip. Rev.: Comput. Mol. Sci.*, 2011, **1**, 211–228.

47 I. Vasiliev, S. Öğüt and J. R. Chelikowsky, *Phys. Rev. Lett.*, 1997, **78**, 4805.

